ACS APPLIED MATERIALS & INTERFACES

Research Article

www.acsami.org

Reversible Conversion-Alloying of Sb_2O_3 as a High-Capacity, High-Rate, and Durable Anode for Sodium Ion Batteries

Meijuan Hu,[†] Yinzhu Jiang,*[,†] Wenping Sun,[‡] Hongtao Wang,[†] Chuanhong Jin,[†] and Mi Yan*[,†]

[†]State Key Laboratory of Silicon Materials, Department of Materials Science and Engineering, Zhejiang University, Hangzhou 310027, China

[‡]School of Materials Science and Engineering, Nanyang Technological University, 50 Nanyang Avenue, Singapore 639798, Singapore

Supporting Information

ABSTRACT: Sodium ion batteries are attracting ever-increasing attention for the applications in large/grid scale energy storage systems. However, the research on novel Na-storage electrode materials is still in its infancy, and the cycling stability, specific capacity, and rate capability of the reported electrode materials cannot satisfy the demands of practical applications. Herein, a high performance Sb_2O_3 anode electrochemically reacted via the reversible conversion-alloying mechanism is demonstrated for the first time. The Sb_2O_3 anode exhibits a high capacity of 550 mAh g^{-1} at 0.05 A g^{-1} and 265 mAh g^{-1} at 5 A g^{-1}. A reversible capacity of 414 mAh g^{-1} at 0.5 A g^{-1} is achieved after 200 stable cycles. The synergistic effect involving conversion and alloying reactions promotes stabilizing the structure of the active material and accelerating the kinetics of the reaction. The mechanism may offer a well-balanced approach for sodium storage to create high capacity and cycle-stable anode materials.

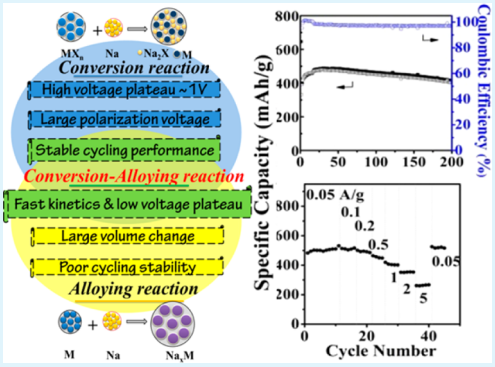

KEYWORDS: *sodium ion battery, anode, Sb_2O_3, conversion, alloying*

1. INTRODUCTION

The increasing demand for low cost, long lifetime, and stable energy storage in applications of large/grid scale energy storage systems (ESSs) has propelled the exploration for alternative battery concepts beyond lithium ion batteries (LIBs).[1−3] Sodium ion batteries (SIBs) have recently attracted worldwide attention owing to the favorable cost performance and the natural sodium abundance.[4−6] Since sodium shares similar chemical properties to lithium, SIBs are currently following the footsteps of LIBs in the research field of electrode materials for sodium storage. In the case of anodes, materials that store sodium via mechanisms of alloying or conversion possess much higher theoretical capacity compared to carbon-based materials, and are now under intensive investigation for accelerating the practical applications of SIBs.[7−12] For the anodes with alloying reactions, the relatively low reaction potential is beneficial for delivering high working voltages of a full cell (Figure 1). The recent work on Sb and Sn/C anode clearly demonstrates even lower average reaction voltage in SIBs than that in LIBs.[13,14] Furthermore, the fast kinetics of alloying reactions can lead to low hysteresis (e.g., only 0.06 V for Sn/C),[14] which is extremely important for making full use of charged energy. Nevertheless, compared to the case in LIBs, the Na alloying/dealloying processes cause much more serious volume change due to the larger size of the Na ion, which results in crack formation and pulverization of active materials and finally fades the electrochemical performance of the electrode.[15] Different from the Na-alloying reactions, the conversion reaction of the anode involves the reversible formation and decomposition of Na_2X (X = O, S, etc.), which acts as a "buffer matrix" for relieving the volume change and brings about stable cycling perform-

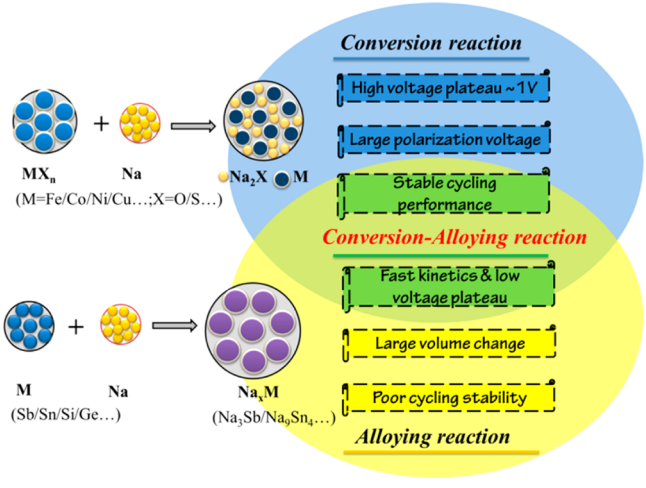

Figure 1. Schematic diagram of the characterstics of the alloying reaction and conversion reaction and their relationship between the alloying-conversion reaction.

Received: August 19, 2014
Accepted: October 20, 2014
Published: October 20, 2014

ances.[7,12,16,17] However, the large voltage hysteresis induced by the sluggish reaction kinetics and the high reaction potential significantly limits their practical utilization in SIBs.[12,18,19] The recent investigation on the SnO_2 electrode of LIBs confirms the higher reversible capacity and prolonged cycling compared to metal Sn owing to the involved reversible conversion reaction with the alloying reaction.[20−22] The successful exploration of ZnM_2O_4 (M = Fe, Mn, Co, etc.) electrodes of LIBs has demonstrated the reversible capacity contribution through both alloy formation and conversion reaction, which leads to high reversible capacity, enhanced cycling stability, and decreased reaction potential.[23−26] Very recent research on the GeO_2−SnCoC electrode of LIBs also demonstrates the facilitated conversion reaction and durable cycling due to the coexistence of conversion and alloying reactions.[27] On the basis of the aforementioned discussion, highly efficient and durable sodium storage might be achieved in anode materials by combining the alloying and conversion reaction mechanisms, as illustrated in Figure 1.

Herein, we successfully demonstrate high sodium storage performance in the Sb_2O_3 electrode, which inserts/extracts sodium ions reversibly via the combined conversion-alloying mechanism. The unique conversion-alloying reactions are found to be superior to the conversion or alloying reaction, as mostly reported in the literature (Figure 1). The Sb_2O_3 anode delivers a high specific charge capacity of 509 mAh g^{-1} at 0.05 A g^{-1}, and retains as high as 265 mAh g^{-1} at a ultrahigh current density of 5 A g^{-1}. The restored capacity could reach 550 mAh g^{-1} at 0.05 A g^{-1} after a rate performance test. In addition to high specific capacity and good rate capability, Sb_2O_3 also exhibits outstanding cycling stability at a high current density of 0.5 A g^{-1}, and a high reversible capacity of 414 mAh g^{-1} is still achieved after 200 cycles.

2. EXPERIMENTAL SECTION

Preparation of Sb_2O_3 Film. With a precursor solution of 0.01 M antimony acetate in ethanol and ethylene glycol (4:1 in volume), Sb_2O_3 thin films were prepared by the electrostatic spray deposition (ESD) technique for 3 h on a stainless steel substrate heated at 160 °C (feeding rate: 2 mL h^{-1}). The distance and the applied voltage between the nozzle and substrate were 4 cm and 7 kV, respectively. The mass of the deposited material was measured using a microbalance with an accuracy of 0.002 mg (Sartorius CPA26P, Germany) before and after deposition.

Characterization. The crystal structure of the film was characterized by powder-XRD with a Rigaku D/max 2550PC X-ray diffractometer. The morphology of the film was observed using scanning electron microscopy (SEM; Hitachi S-4800, Tokyo, Japan). The crystal structure details were further characterized by transmission electron microscopy (TEM; Tecnai G2 F20 S-TWIN, FEI, America). X-ray photoelectron spectroscopic (XPS) measurements were performed with an ESCALAB 250 X-ray photoelectron spectrometer, using an excitation energy of 1486.6 eV (Al Kα).

Electrochemical Measurements. The electrochemical behavior was examined in CR2025 coin-type cells using the as-deposited films on stainless steel substrate as the working electrode and sodium foil as the counter and reference electrode, respectively. Cell assembling was carried out in an argon filled glovebox, in which the oxygen concentration and moisture level were maintained at less than 1 ppm. Celgard 2300 microporous polypropylene was used as a separator. The electrolyte was 1 M $NaPF_6$ in a mixture solvent of ethylene carbonate (EC), diethyl carbonate (DEC), and propylene carbonate (PC) (4:4:2 by volume) with 5% fluoroethylene carbonate (FEC) added.[13,28,29] The cells were charged and discharged galvanostatically on a Neware BTS battery cycler at 0.01−2.0 V (vs Na/Na^+). Cyclic voltammetry (CV) tests were conducted on a CHI660C electrochemistry workstation between 0.01 and 2.0 V (vs Na/Na^+) at 0.1 mV s^{-1}.

3. RESULTS AND DISCUSSION

The present Sb_2O_3 film electrode was directly deposited by electrostatic spray deposition (ESD), which is a facile technique to prepare high-performance electrode films for batteries. As shown in the XRD pattern of the Sb_2O_3 film (Figure 2a), all the

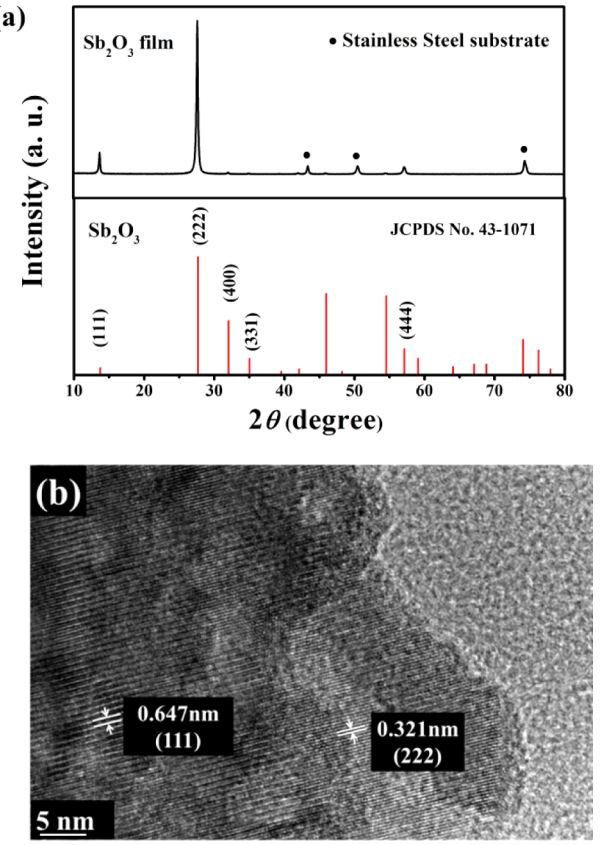

Figure 2. (a) XRD pattern and (b) high resolution TEM image of synthesized Sb_2O_3 film.

diffraction peaks correspond to cubic Sb_2O_3 (JCPDS No. 43-1071) except for the substrate peaks. The film consisted of irregular polygon particles with a size that ranged from 0.2 to 0.5 μm and with an average thickness of around 0.7 μm (Figure S1, Supporting Information). The relative uncompact structure of the film ensures the full infiltration of the electrolyte solution and promotes the migration of the sodium ions. Figure 2b shows the high resolution transmission electron microscopy (HR-TEM) (Figure 2b) image of the Sb_2O_3 grains scratched from the substrate. The two lattice fringes with basal distances of 0.647 and 0.321 nm correspond to the (111) and (222) planes of cubic Sb_2O_3, respectively, which is well consistent with the XRD result.

Electrochemical Na-storage performances of the Sb_2O_3 electrode are given in Figure 3. As shown in Figure 3a, the cyclic voltammetry (CV) profile of the first scan is distinctively different from the subsequent scans, indicating that there is an activation step during the first discharge/charge process.[5] During the second and third scans, the anodic and cathodic profiles are well overlapped, indicating the high reversibility and good capacity retention of the electrode. The Sb_2O_3 electrode shows a sloping reduction peak at 0.87 V and a symmetric

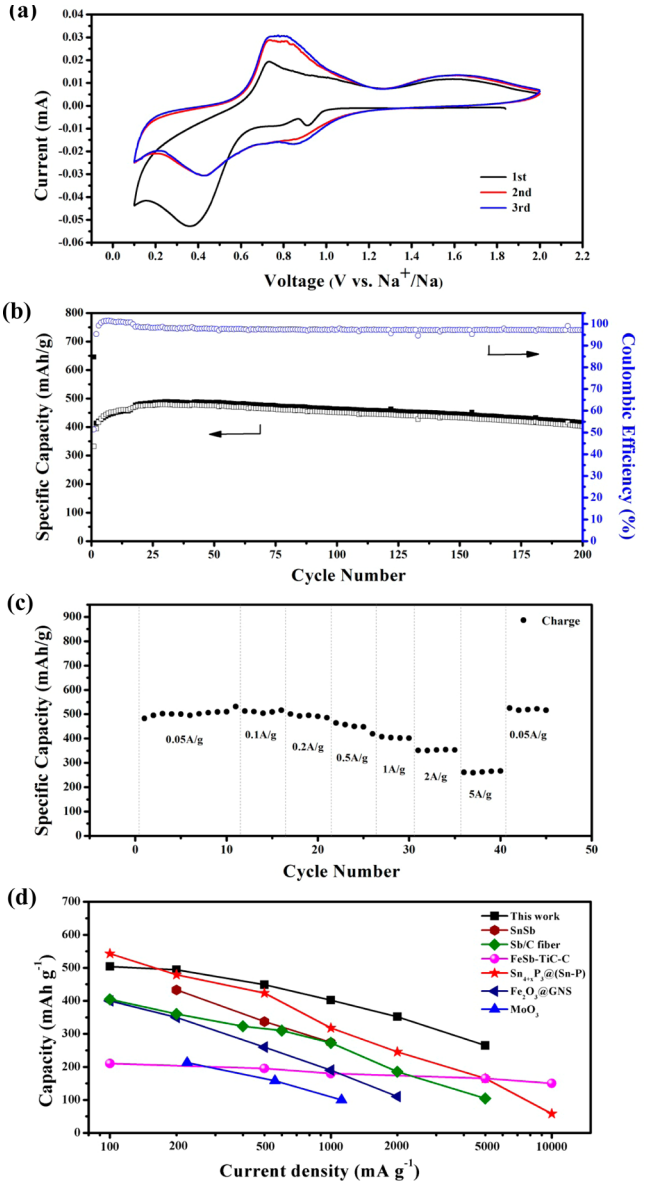

Figure 3. (a) Cyclic voltammetry profiles of Sb_2O_3 electrode at a scan rate of 0.1 mV s^{-1} for the first three cycles within a potential range of 0.01−2.0 V (vs Na/Na^+). (b) Cycling performance of Sb_2O_3 at a current density of 0.5 A g^{-1}. (c) Rate performance of the Sb_2O_3 electrode at different current rates. (d) A comparison of the rate capacity of Sb_2O_3 with alloying material and conversion type materials.

reduction peak at 0.42 V, corresponding to the wide oxidation peak in the range 1.25−2.0 V and another anodic peak at 0.77 V. These two pairs of redox peaks are probably attributed to the conversion and alloying reactions, respectively. Figure 3b presents the cycling performance of the Sb_2O_3 electrode at a current density of 0.5 A g^{-1}. The first discharge and charge capacity of the Sb_2O_3 electrode is 645 and 331 mAh g^{-1}, respectively, corresponding to a Columbic efficiency of only 51.3%. The relatively low initial Coulombic efficiency is frequently observed in the alloying-type anodes, and the irreversible capacity is possible due to the electrolyte decomposition and the formation of a solid electrolyte interface (SEI) on the electrode surface. The Coulombic efficiency has been greatly increased to around 95% in the second cycle, indicating that such irreversible reactions are significantly diminished, which might be due to the stabilized SEI layer. The reversible capacity gradually increases with cycling in the first 30 cycles, suggesting the existence of an activation process for sodiation/desodiation. Impressively, the Sb_2O_3 electrode can still deliver a capacity up to 414 mAh g^{-1} after 200 cycles with a high Coulombic efficiency of 97.2%. Rate capability is critical for achieving fast charge/discharge batteries. As shown in Figure 3c, the Sb_2O_3 electrode delivers specific capacities of 509, 504, 494, 449, 402, 352, and 265 mAh g^{-1} at current densities of 0.05, 0.1, 0.2, 0.5, 1.0, 2.0, and 5.0 A g^{-1}, respectively. The specific capacity at an ultralarge current density of 5.0 A g^{-1} exceeds that of most SIB anodes reported previously. Meantime, as high as ∼550 mAh g^{-1} of reversible capacity is restored when the current density is switched from 5 to 0.05 A g^{-1}. The rate performance of Sb_2O_3 is also compared with those of reported tin or antimony based composites (Sb/C,[29] SnSb/C,[30] FeSb-TiC-C,[31] $Sn_{4+x}P_3$@(Sn−P)[8]) in the form of alloying, together with the transitional metal oxides (Fe_2O_3@GNS,[18] α-MoO_3[32]) through conversion reactions, as shown in Figure 3d. Even though most of the compared anode materials are carefully structured or composition-engineered for the enhanced electrochemical performances, it is clear that the rate capability of Sb_2O_3 is superior to most of the cited anode materials, demonstrating that Sb_2O_3 has a great potential working as a high-performance material for sodium storage. It can be anticipated that the sodium storage performance would be further enhanced by designing more efficient and stable microstructures of Sb_2O_3.

To understand the impressive electrochemical performance and determine the exact sodiation/desodiation mechanism with the Sb_2O_3 electrode, comprehensive *ex situ* measurements including XRD, HR-TEM, selected area electron diffraction (SAED), and X-ray photospectroscopy (XPS) were performed at various charged/discharged states between 0.01 and 2.0 V at a low current of 10 mA g^{-1}, as shown in Figure 4. Although a considerable Na-storage capacity is recorded after being discharged to 0.8 V, all the diffraction peaks can still be attributed to the cubic Sb_2O_3 phase except for the substrate peaks. In comparison with the XRD pattern of the pristine Sb_2O_3, there is a slight shift to low angle for all characteristic peaks (Figure 4c), suggesting a lattice expansion of the Sb_2O_3 crystal structure. On the basis of the HR-TEM image of Sb_2O_3 (Figure 4d), the lattice spacing of the (111) crystal plane increased from 0.647 to 0.650 nm after being discharged to 0.8 V, confirming the lattice expansion behavior. Thus, it can be deduced that the Na storage capacity at a potential higher than 0.8 V should come from Na intercalation into Sb_2O_3. A small amount of sodium can be inserted into the crystal structure of cubic Sb_2O_3 without a change in structure, which was also found in the SnO_2 anode.[33] The diffraction peaks of cubic Sb_2O_3 disappear completely when the electrode is discharged to 0.4 V, while no other diffraction peaks are present. This might result from the decomposition of Sb_2O_3 and the formation of nanocrystalline metal Sb. More details can be obtained in the corresponding HR-TEM image (Figure 4e). The lattice spacing of 0.375 nm can be assigned to the (003) plane of Sb. In addition, the hexagonal spots of the SAED pattern can be well indexed along the [010] zone axis of Sb. On the basis of the above results, we can conclude that Sb_2O_3 has been reduced to Sb completely at this discharged state, accompanied by the formation of Na_2O. When fully discharged to 0.01 V, most of the diffraction peaks can be assigned to the $NaSb(OH)_6$ phase, implying the formation of the NaSb alloy phase (Figure 4b).

dx.doi.org/10.1021/am505505m | ACS Appl. Mater. Interfaces 2014, 6, 19449−19455

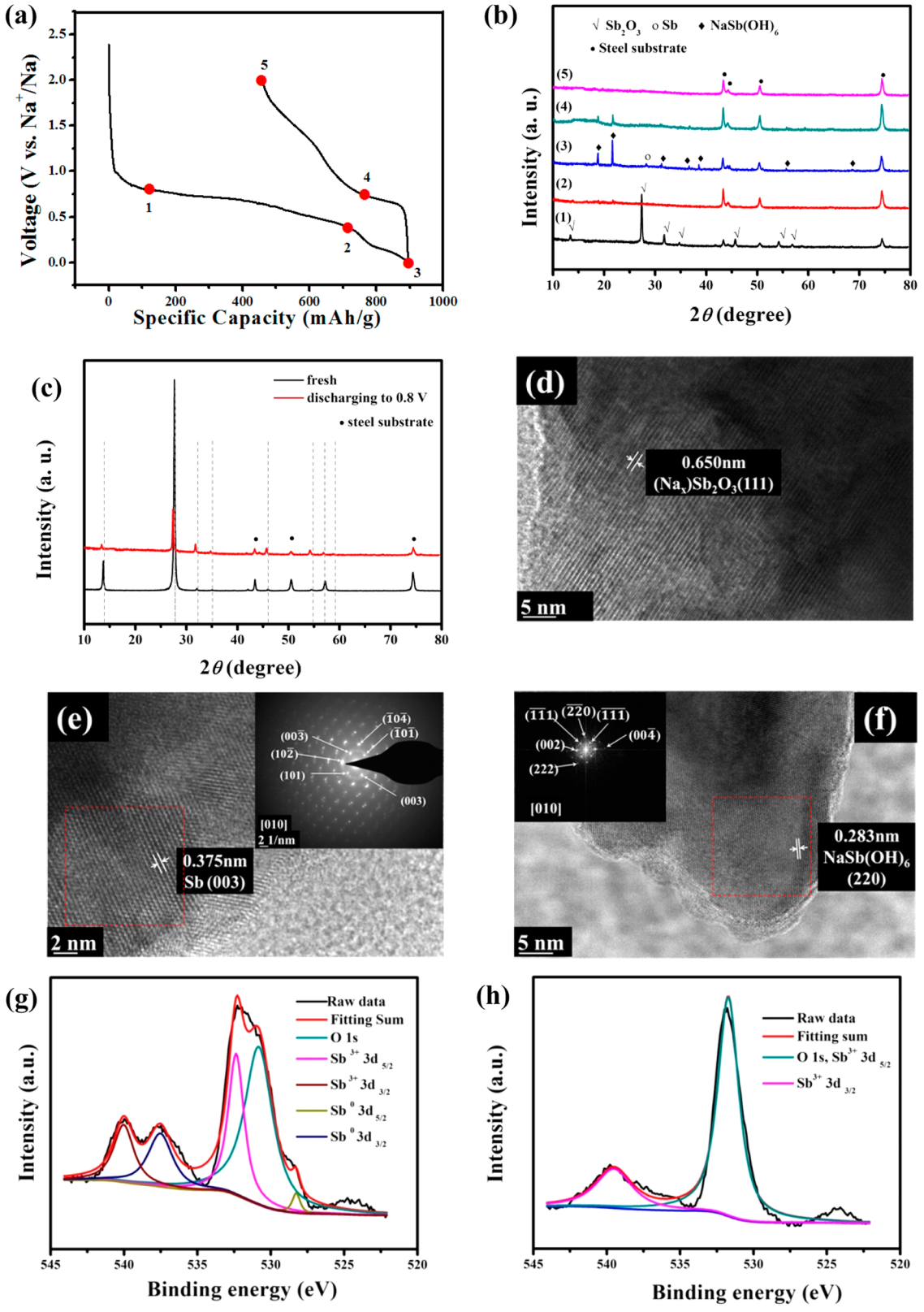

Figure 4. (a) Charge–discharge curves of the Sb_2O_3 electrode at a current density of 10 mA g^{-1} during the first cycle. (b) The XRD patterns of the film electrodes (1) after the first discharge to 0.8 V, (2) after the first discharge to 0.4 V, (3) after the first discharge to 0.01 V, (4) after the first charge to 0.75 V, and (5) after the first charge to 2 V. (c) The XRD patterns of the film electrode after the first discharge to 0.8 V compared with fresh Sb_2O_3 film. *Ex situ* TEM images of the film electrodes (d) after the first discharge to 0.8 V, (e) after the first discharge to 0.4 V (the inset is the corresponding SAED pattern), and (f) after the first discharge to 0.01 V (the inset is the corresponding FFT pattern). XPS spectra of Sb 3d and O 1s of the film electrodes (g) after the first charge to 0.75 V and (h) after the first charge to 2.0 V.

dx.doi.org/10.1021/am505505m | *ACS Appl. Mater. Interfaces* 2014, 6, 19449–19455

Consistently, the lattice spacing of 0.283 nm corresponds to the (220) plane of $NaSb(OH)_6$ (Figure 4f). The fast Fourier transforms (FFTs) in the inset can also be indexed as a tetragonal phase viewed along the [010] zone axis of mopungite. The existence of $NaSb(OH)_6$ is probably due to the unavoidable reactions between the discharge product of NaSb with water and oxygen during the transferring process.[14] It is worthwhile to note, different from the appearance of Na_3Sb in the metal Sb anode reported in the literature, only NaSb alloy is formed during the present alloying reaction. In the following charge to 0.75 and 2 V, no crystalline peaks can be observed in the XRD patterns except for substrate peaks, suggesting that the material becomes amorphous; meanwhile, the amorphous characteristic is also confirmed by the TEM results (Figure S2, Supporting Information). In order to ascertain the phase composition of the product, *ex situ* XPS was conducted for the charged samples by identifying the valence state of the Sb element, which is shown in Figure 4g and h. In the charged state at 0.75 V, Sb(III) peaks at 540.0 and 530.6 eV as well as elemental Sb(0) peaks at 537.5 and 528.2 eV can be distinguished, confirming the existence of both Sb_2O_3 and metallic antimony in the film. When charged back to 2.0 V, only Sb(III) peaks can be inferred in Figure 4h, which demonstrates the reversible oxidation of Sb to Sb_2O_3 after being fully charged.

According to the analysis above, the electrochemical reaction mechanism of Sb_2O_3 with sodium is in accordance with the combined conversion-alloying reactions:

$$Sb_2O_3 + xNa^+ + xe^- \rightarrow Na_xSb_2O_3 \qquad \text{(1st discharge)} \tag{1}$$

$$Na_xSb_2O_3 + (6 - x)Na^+ + (6 - x)e^- \rightarrow 2Sb + 3Na_2O \qquad \text{(1st discharge)} \tag{2}$$

$$Sb_2O_{3(\text{amorphous})} + 6Na^+ + 6e^- \leftrightarrow 2Sb + 3Na_2O \qquad \text{(after 1st cycle)} \tag{3}$$

$$Sb + Na^+ + e^- \leftrightarrow NaSb \tag{4}$$

In the initial cycle, Na ion first intercalates into the Sb_2O_3 crystal structure, leading to the formation of $Na_xSb_2O_3$ in the potential range of 0.6−1.0 V. The small peak at 0.92 V in the first anodic scan of the CV test could be assigned to the intercalation behavior of Na ion, which does not occur in the subsequent cycles due to the breakdown of the Sb_2O_3 cubic structure after the first cycle. In the second step, the conversion of $Na_xSb_2O_3$ into Sb and Na_2O is confirmed by the formation of antimony. As suggested above, the conversion reaction after the first cycle will be conducted directly with Sb_2O_3, as proposed in eq 3. It can be concluded that the redox pair peak of 0.87 V/1.25−2 V in the CV profiles can be assigned to the reversible conversion reaction. Similar conversion phenomena have been reported in the research of MoO_3 and Fe_2O_3 electrodes of SIBs.[12,32] The following stage involves Na-alloying reaction of Sb into NaSb, and this is different from the metal Sb anode, where Na_3Sb alloy is produced.[13,34] The research on the Sb_2S_3 anode also reveals the same alloying product.[9] Furthermore, the shape of the charge−discharge profiles and voltage plateau during the subsequent cycles were kept almost the same (Figure S3, Supporting Information), indicating a unique and reversible reaction mechanism. The above results clearly demonstrate the reversible combined conversion-alloying reaction mechanism in the case of the Sb_2O_3 electrode of SIBs.

If we assume the final discharge product is NaSb based on the *ex situ* characterization, a complete conversion-alloying reaction will involve a total of 8 Na atoms per formula unit, resulting in a theretical capacity of 735 mAh g^{-1}. Combined with the first charge/discharge profiles of Sb_2O_3 at 10 mAg^{-1}, three reaction stages contribute to a first discharge capacity of 894 mAh g^{-1}, which is higher than the above theoretical capacity. If conversion and alloying reactions fully occur under such a low current density of 10 mA g^{-1}, an extra capacity of 159 mAh g^{-1} is possibly originated from the additional Na consumption on the electrolyte decomposition and the SEI formation. However, the first charge capacity is only 435 mAh g^{-1}, indicating there are some irreversible reactions and/or a necessary activation process considering the microscale size of Sb_2O_3 particles. Furthermore, when the current density increases to 500 mA g^{-1}, the first discharge and charge capacity are only 645 and 331 mAh g^{-1}, respectively, suggesting about a half amount of active material is not reversibly reacted in the early peirod of the cycling process. This might be the polarization effect induced by the low electron/Na^+ conduction of conductive agent-free electrode and microscale size of Sb_2O_3 particles. Along with cycling, the specific capacity has gradually increased to 485 mAh g^{-1}, indicating more active materials involved, which might be due to the electrochemical grinding and activation effect. According to the analysis above, combining with the high electric conductivity material such as carbon or nanosizing the Sb_2O_3 particle can improve the utilization of active material and thus increase the specific capacity.

The outstanding electrochemical performance of Sb_2O_3 can be ascribed to the conversion-alloying reaction between Sb_2O_3 and Na. First, the continuous and amorphous Na_2O generated in the conversion reaction acts as a perfect buffer for the following alloying reaction, effectively relieving the stress associated with the volume change and preventing the particle agglomeration. Second, compared to the single conversion mechanism, the extra alloying reaction will help to accelerate the reaction kinetics and drag down the average electrochemical potential plateau. Third, the combined conversion-alloying electrochemical reactions could involve more sodium ions and deliver a higher specific capacity and energy density. Overall, the synergistic effect involving conversion and alloying reactions promotes stabilizing the structure of the active material and accelerating the kinetics of the reaction. Additionally, we could anticipate even a much higher specific capacity if the final alloying product can be designed as Na_3Sb, not the present case of NaSb. Nanostructuring/compositing the Sb_2O_3 active materials is a possible way[9,29,34−36] through which the chemical state or electrical conductivity can be changed, leading to improved electrochemical performance.

4. CONCLUSIONS

In summary, we demonstrate combined conversion-alloying electrochemical reactions in Sb_2O_3, which performs as a high-capacity, high-rate, and durable anode for SIBs. Under the unique Na-storage mechanism, the Sb_2O_3 electrode delivers a high charge capacity of 509 mAh g^{-1} at 0.05 A g^{-1}, and retains as high as 265 mAh g^{-1} at an ultrahigh current density of 5 A g^{-1}. Furthermore, an outstanding cycling stability is also demonstrated with a reversible capacity of 414 mAh g^{-1} at 0.5 A g^{-1} after 200 stable cycles. The reversible combined

conversion-alloying mechanism might offer well-balanced sodium storage to create high-capacity and cycle-stable anode materials.

■ ASSOCIATED CONTENT

Supporting Information

SEM images of the surface and cross section morphology of pristine Sb_2O_3 film, *ex situ* TEM images and the corrresponding SAED patterns of the film electrodes after the first charge to 0.75 and 2.0 V, the charge−discharge voltage profiles of the 1st, 5th, 10th, 20th, and 50th cycles for the Sb_2O_3 electrode at a current density of 0.5 A g^{-1}. This material is available free of charge via the Internet at http://pubs.acs.org.

■ AUTHOR INFORMATION

Corresponding Authors

*E-mail: yzjiang@zju.edu.cn.
*E-mail: mse_yanmi@zju.edu.cn.

Notes

The authors declare no competing financial interest.

■ ACKNOWLEDGMENTS

This work was supported by National Natural Science Foundation of China (NSFC-21373184) and Doctoral Fund of Ministry of Education of China. Y.J. wishes to acknowledge an equipment subsidy offered by Alexander von Humboldt (AvH) Foundation. The work on microscopy was carried out in the Center of Electron Microscopy of Zhejiang University.

■ REFERENCES

(1) Tomabechi, K. Energy Resources in the Future. *Energies* **2010**, *3*, 686−695.

(2) Winter, M.; Brodd, R. J. What Are Batteries, Fuel Cells, and Supercapacitors? *Chem. Rev.* **2004**, *104*, 4245−4269.

(3) Barnhart, C. J.; Benson, S. M. On the Importance of Reducing the Energetic and Material Demands of Electrical Energy Storage. *Energy Environ. Sci.* **2013**, *6*, 1083−1092.

(4) Palomares, V.; Casas-Cabanas, M.; Castillo-Martinez, E.; Han, M. H.; Rojo, T. Update on Na-based Battery Materials. A Growing Research Path. *Energy Environ. Sci.* **2013**, *6*, 2312−2337.

(5) Slater, M. D.; Kim, D.; Lee, E.; Johnson, C. S. Sodium-Ion Batteries. *Adv. Funct. Mater.* **2013**, *23*, 947−958.

(6) Kim, S. W.; Seo, D. H.; Ma, X. H.; Ceder, G.; Kang, K. Electrode Materials for Rechargeable Sodium-Ion Batteries: Potential Alternatives to Current Lithium-Ion Batteries. *Adv. Energy Mater.* **2012**, *2*, 710−721.

(7) Qu, B.; Ma, C.; Ji, G.; Xu, C.; Xu, J.; Meng, Y. S.; Wang, T.; Lee, J. Y. Layered SnS_2-Reduced Graphene Oxide Composite - A High-Capacity, High-Rate, and Long-Cycle Life Sodium-Ion Battery Anode Material. *Adv. Mater.* **2014**, *26*, 3854−3859.

(8) Li, W.; Chou, S. L.; Wang, J. Z.; Kim, J. H.; Liu, H. K.; Dou, S. X. $Sn_{4+x}P_3$ @ Amorphous Sn-P Composites as Anodes for Sodium-Ion Batteries with Low Cost, High Capacity, Long Life, and Superior Rate Capability. *Adv. Mater.* **2014**, *26*, 4037−4042.

(9) Yu, D. Y.; Prikhodchenko, P. V.; Mason, C. W.; Batabyal, S. K.; Gun, J.; Sladkevich, S.; Medvedev, A. G.; Lev, O. High-capacity Antimony Sulphide Nanoparticle-decorated Graphene Composite as Anode for Sodium-ion Batteries. *Nat. Commun.* **2013**, *4*, 2922.

(10) Yuan, S.; Huang, X. L.; Ma, D. L.; Wang, H. G.; Meng, F. Z.; Zhang, X. B. Engraving Copper Foil to Give Large-Scale Binder-Free Porous CuO Arrays for a High-Performance Sodium-Ion Battery Anode. *Adv. Mater.* **2014**, *26*, 2273−2279.

(11) Qian, J. F.; Xiong, Y.; Cao, Y. L.; Ai, X. P.; Yang, H. X. Synergistic Na-storage Reactions in Sn_4P_3 as a High-capacity, Cycle-stable Anode of Na-ion Batteries. *Nano Lett.* **2014**, *14*, 1865−1869.

(12) Jiang, Y. Z.; Hu, M. J.; Zhang, D.; Yuan, T. Z.; Sun, W. P.; Xu, B.; Yan, M. Transition Metal Oxides for High Performance Sodium iIon Battery Anodes. *Nano Energy* **2014**, *5*, 60−66.

(13) Darwiche, A.; Marino, C.; Sougrati, M. T.; Fraisse, B.; Stievano, L.; Monconduit, L. Better Cycling Performances of Bulk Sb in Na-ion Batteries Compared to Li-ion Systems: an Unexpected Electrochemical Mechanism. *J. Am. Chem. Soc.* **2012**, *134*, 20805−20811.

(14) Xu, Y. H.; Zhu, Y. J.; Liu, Y. H.; Wang, C. S. Electrochemical Performance of Porous Carbon/Tin Composite Anodes for Sodium-Ion and Lithium-Ion Batteries. *Adv. Energy Mater.* **2013**, *3*, 128−133.

(15) Wang, J. W.; Liu, X. H.; Mao, S. X.; Huang, J. Y. Microstructural Evolution of Tin Nanoparticles during In Situ Sodium Insertion and Extraction. *Nano Lett.* **2012**, *12*, 5897−5902.

(16) Sun, Q.; Ren, Q. Q.; Li, H.; Fu, Z. W. High Capacity Sb_2O_4 Thin Film Electrodes for Rechargeable Sodium Battery. *Electrochem. Commun.* **2011**, *13*, 1462−1464.

(17) Xie, X. Q.; Su, D. W.; Chen, S. Q.; Zhang, J. Q.; Dou, S. X.; Wang, G. X. SnS_2 Nanoplatelet@Graphene Nanocomposites as High-Capacity Anode Materials for Sodium-Ion Batteries. *Chem.—Asian J.* **2014**, *9*, 1611−1617.

(18) Jian, Z. L.; Zhao, B.; Liu, P.; Li, F. J.; Zheng, M. B.; Chen, M. W.; Shi, Y.; Zhou, H. S. Fe_2O_3 Nanocrystals Anchored onto Graphene Nanosheets as the Anode Material for Low-cost Sodium-ion Batteries. *Chem. Commun.* **2014**, *50*, 1215−1217.

(19) Valvo, M.; Lindgren, F.; Lafont, U.; Björefors, F.; Edström, K. Towards More Sustainable Negative Electrodes in Na-ion Batteries via Nanostructured Iron Oxide. *J. Power Sources* **2014**, *245*, 967−978.

(20) Wang, D. N.; Yang, J. L.; Li, X. F.; Geng, D. S.; Li, R. Y.; Cai, M.; Sham, T. K.; Sun, X. L. Layer by Layer Assembly of Sandwiched Graphene/SnO_2 Nanorod/carbon Nanostructures with Ultrahigh Lithium Ion Storage Properties. *Energy Environ. Sci.* **2013**, *6*, 2900−2906.

(21) Li, X. F.; Meng, X. B.; Liu, J.; Geng, D. S.; Zhang, Y.; Banis, M. N.; Li, Y. L.; Yang, J. L.; Li, R. Y.; Sun, X. L.; Cai, M.; Verbrugge, M. W. Tin Oxide with Controlled Morphology and Crystallinity by Atomic Layer Deposition onto Graphene Nanosheets for Enhanced Lithium Storage. *Adv. Funct. Mater.* **2012**, *22*, 1647−1654.

(22) Zhang, B. A.; Yu, Y.; Huang, Z. D.; He, Y. B.; Jang, D.; Yoon, W. S.; Mai, Y. W.; Kang, F. Y.; Kim, J. K. Exceptional Electrochemical Performance of Freestanding Electrospun Carbon Nanofiber Anodes Containing Ultrafine SnO_x Particles. *Energy Environ. Sci.* **2012**, *5*, 9895−9902.

(23) Deng, Y. F.; Zhang, Q. M.; Tang, S. D.; Zhang, L. T.; Deng, S. N.; Shi, Z. C.; Chen, G. H. One-pot Synthesis of $ZnFe_2O_4$/C Hollow Spheres as Superior Anode Materials for Lithium Ion Batteries. *Chem. Commun.* **2011**, *47*, 6828−6830.

(24) Sharma, Y.; Sharma, N.; Rao, G. V. S.; Chowdari, B. V. R. Nanophase $ZnCo_2O_4$ as a High Performance Anode Material for Li-Ion Batteries. *Adv. Funct. Mater.* **2007**, *17*, 2855−2861.

(25) Liu, B.; Zhang, J.; Wang, X. F.; Chen, G.; Chen, D.; Zhou, C. W.; Shen, G. Z. Hierarchical Three-Dimensional $ZnCo_2O_4$ Nanowire Arrays/Carbon Cloth Anodes for a Novel Class of High-Performance Flexible Lithium-Ion Batteries. *Nano Lett.* **2012**, *12*, 3005−3011.

(26) Zhang, G. Q.; Yu, L.; Wu, H. B.; Hoster, H. E.; Lou, X. W. Formation of $ZnMn_2O_4$ Ball-in-Ball Hollow Microspheres as a High-Performance Anode for Lithium-Ion Batteries. *Adv. Mater.* **2012**, *24*, 4609−4613.

(27) Liu, B.; Abouimrane, A.; Balasubramanian, M.; Ren, Y.; Amine, K. GeO_2−SnCoC Composite Anode Material for Lithium-Ion Batteries. *J. Phys. Chem. C* **2014**, *118*, 3960−3967.

(28) Wang, Z. H.; Qie, L.; Yuan, L. X.; Zhang, W. X.; Hu, X. L.; Huang, Y. H. Functionalized N-doped Interconnected Carbon Nanofibers as an Anode Material for Sodium-ion Storage with Excellent Performance. *Carbon* **2013**, *55*, 328−334.

(29) Zhu, Y. J.; Han, X. G.; Xu, Y. H.; Liu, Y. H.; Zheng, S. Y.; Xu, K.; Hu, L. B.; Wang, C. S. Electrospun Sb/C Fibers for a Stable and Fast Sodium-Ion Battery Anode. *ACS Nano* **2013**, *7*, 6378−6386.

(30) Xiao, L. F.; Cao, Y. L.; Xiao, J.; Wang, W.; Kovarik, L.; Nie, Z. M.; Liu, J. High Capacity, Reversible Alloying Reactions in SnSb/C

Nanocomposites for Na-ion Battery Applications. *Chem. Commun.* **2012**, *48*, 3321−3323.
(31) Kim, I. T.; Allcorn, E.; Manthiram, A. High-performance FeSb−TiC−C Nanocomposite Anodes for Sodium-ion Batteries. *Phys. Chem. Chem. Phys.* **2014**, *16*, 12884−12889.
(32) Hariharan, S.; Saravanan, K.; Balaya, P. α-MoO_3: A High Performance Anode Material for Sodium-ion Batteries. *Electrochem. Commun.* **2013**, *31*, 5−9.
(33) Su, D. W.; Wang, C. Y.; Ahn, H.; Wang, G. X. Octahedral Tin Dioxide Nanocrystals as High Capacity Anode Materials for Na-ion Batteries. *Phys. Chem. Chem. Phys.* **2013**, *15*, 12543−12550.
(34) Qian, J. F.; Chen, Y.; Wu, L.; Cao, Y. L.; Ai, X. P.; Yang, H. X. High Capacity Na-storage and Superior Cyclability of Nanocomposite Sb/C Anode for Na-ion Batteries. *Chem. Commun.* **2012**, *48*, 7070−7072.
(35) Farbod, B.; Cui, K.; Kalisvaart, W. P.; Kupsta, M.; Zahiri, B.; Kohandehghan, A.; Lotfabad, E. M.; Li, Z.; Luber, E. J.; Mitlin, D. Anodes for Sodium Ion Batteries Based on Tin-Germanium-Antimony Alloys. *ACS Nano* **2014**, *8*, 4415−4429.
(36) Baggetto, L.; Allcorn, E.; Manthiram, A.; Veith, G. M. Cu_2Sb thin films as anode for Na-ion batteries. *Electrochem. Commun.* **2013**, *27*, 168−171.